

# Analysis of aerodynamic characteristics on a counter-rotating wind turbine

Seungmin Lee<sup>a,\*</sup>, Hogeon Kim<sup>a</sup>, Soogab Lee<sup>b</sup>

<sup>a</sup>Department of Mechanical and Aerospace Engineering, Seoul National University, Seoul 151-742, Republic of Korea

<sup>b</sup>Institute of Advanced Aerospace Technology, Department of Mechanical and Aerospace Engineering, Seoul National University, Seoul 151-744, Republic of Korea

## ARTICLE INFO

### Article history:

Received 5 December 2008

Accepted 9 June 2009

Available online 12 November 2009

### Keywords:

Counter-rotating wind turbine

Vortex lattice method

Equal solidity

## ABSTRACT

This study aims to analyze aerodynamic characteristics of a counter-rotating wind turbine. For this purpose, three kinds of rotor configurations which are 2-bladed single, 4-bladed single and counter-rotating rotor were compared by using a numerical method. The numerical method used here was based on vortex lattice method and was validated with measurements of the NREL phase-VI rotor. Through numerical calculations of induction factors and power coefficients for each rotor configuration, the aerodynamic feasibility of a counter-rotating wind turbine was considered.

© 2009 Elsevier B.V. All rights reserved.

## 1. Introduction

Wind is one of the clean energy sources, and its conversion to usable energy is important to reduce fossil fuel dependency. In order to obtain energy from wind, a lot of wind turbines are being constructed. However, regions having high wind energy density are finite. Therefore, many researches to increase energy efficiency of wind turbines have been accomplished.

Generally, horizontal axis wind turbines (HAWT) having a single rotor is used for conventional wind turbine systems. According to Betz theory [1], the maximum energy conversion efficiency of conventional wind turbines having a single rotor is about 59%. By contrast, the maximum efficiency obtained by two rotors having the same area is increased to 64% [2]. Based on this results, in order to increase the energy efficiency of wind turbines, some researches for counter-rotating wind turbines (CRWT) that have two rotors rotating opposite direction at the same axis have been progressed.

Appa Technology Initiatives [3] has established a proto model of 6 kW CRWT in California. The rotor performance data have been measured and numerical predictions using BEM (blade element-momentum) method have been accomplished. Jung et al. [4] has constructed a 30 kW CRWT system and has obtained power curve experimentally and numerically. In addition, the effects of distance and diameter ratio between two rotors have been considered by using BEM method. Shen et al. [5] has used CFD code, EllipSys3D, to predict performance of a CRWT having two Nordtank 500 kW rotors.

All these researches mentioned above have compared the performance of a CRWT with that of single rotor having half number of blades. However, these comparisons are unfair because each rotor configuration has different solidity (the ratio of total blade area to rotor disk area). In this study, for a fair comparison, aerodynamic characteristics of a CRWT were compared with that of a single rotor having equal solidity as well as a single rotor having half solidity. Through numerical calculations of induction factors and power coefficients for each rotor configuration, the aerodynamic feasibility of a CRWT was considered.

## 2. Numerical method

The numerical method used here is the free wake vortex lattice method. If the flow around wind turbine rotor blades is considered to be incompressible and irrotational, the continuity equation reduces to the Laplace's equation in terms of the total velocity potential,  $\Phi^*$ .

Using the Green's identity, the general solution of the above equation is expressed by a sum of source and doublet distribution placed on a boundary. Following the small disturbance assumption, rotor blades could be replaced with vortex sheets. Therefore the general solution is constructed by following form

$$\Phi^* = \frac{1}{4\pi} \int_{body+wake} \gamma n \cdot \nabla \left( \frac{1}{r} \right) dS + \Phi_\infty. \quad (1)$$

If the direct zero normal velocity condition for the solid surface (Neumann boundary condition) applies to each sub-divided panel, then vortex strength,  $\gamma$ , can be computed by solving a linear matrix equation. The force generated by a vortex sheet is determined by the Kutta–Joukowski theorem (see more details in Ref. [6]).

\* Corresponding author. Fax: +82 2 876 4360.  
E-mail address: [vitamin1@snu.ac.kr](mailto:vitamin1@snu.ac.kr) (S. Lee).

The viscous drag force which is impossible to consider in potential based solver is calculated by using two-dimensional aerodynamic coefficient table. Besides, for a free wake analysis, the velocity induced on the wake panel is calculated and each wake panel is convected using this velocity every time step. In addition, to avoid a singularity of the solution, vortex core radius set to 1% of rotor radius is used.

In order to evaluate flow field induced by a wind turbine, two induction factors were used. First one is the wake axial induction factor and defined as following

$$a_{wake} = 1 - \left( \frac{V_{wake}}{V_{wind}} \right), \tag{2}$$

where  $V_{wake}$  is a wind direction component of induced velocity and  $V_{wind}$  is wind speed. The wake axial induction factor show that the wake state was completely within the windmill state [7]. Second one is the wake angular induction factor which is defined as the ratio of wake swirl velocity,  $\omega_{wake}$ , to angular velocity of a rotor,  $\Omega$ . Thus,

$$a'_{wake} = \frac{\omega_{wake}}{\Omega} = \frac{(v_{\theta})_{wake}}{\Omega r}. \tag{3}$$

Finally, wind turbine performance is characterized by power coefficient, as given below

$$C_p = \frac{P}{\frac{1}{2} \rho (V_{wind})^2 A}. \tag{4}$$

### 3. Results and discussion

#### 3.1. Validation of numerical method

For a validation of the numerical method, shaft torque of the NREL's phase-VI rotor for zero-yaw condition was computed and compared to measurements [8]. The phase-VI rotor of NREL has two blades of 10 m diameter and its solidity is 0.061. The rotor speed and blade pitch angle is 72 rpm and 3°, respectively.

The comparison of the shaft torque as a function of wind speed is shown in Fig. 1. For wind speeds up to about 9 m/s predicted results agree well with measurements. At high wind speeds, however, numerical results give an over-estimation. This discrepancy is related to stalled flow. For the wind speeds larger than 9 m/s the flow on a rotor blade is stalled. Because the numerical method used here is based on the potential flow it has a difficulty to predict stalled flow. Therefore, this study is limited to the wind speed condition in which flow is fully attached.

#### 3.2. Comparison of rotor configurations

For the feasibility study of a CRWT three kinds of rotor configurations were compared by using the numerical method. Fig. 2 describes each rotor configuration. One is a single rotor having two blades and its solidity is 0.061, as shown in Fig. 2a. Another is a 4-bladed single rotor, as shown in Fig. 2b. Its solidity is 0.122, twice of the 2-bladed single rotor. The other is a counter-rotating rotor, as shown in Fig. 2c. It has two rotors rotating opposite direction at the same axis and has equal solidity of 4-bladed single rotor because each rotor has two blades. The ratio of distance between front and rear rotor to rotor diameter (H/D) is 0.1 (for convenience sake, 2S, 4S and 2 × 2C represent 2-bladed single, 4-bladed single and counter-rotating rotor, respectively).

For the comparison the NREL's phase-VI rotor blades were used and both pitch angle and rotor speed were fixed for all configurations. In addition, in order to consider for only attached flow condition, the tip speed ratio (TSR) was restricted to be more than 4.0.

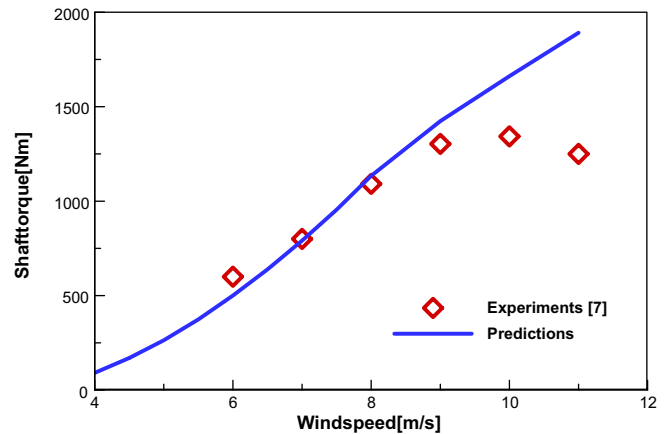


Fig. 1. Shaft torque as function of wind speed.

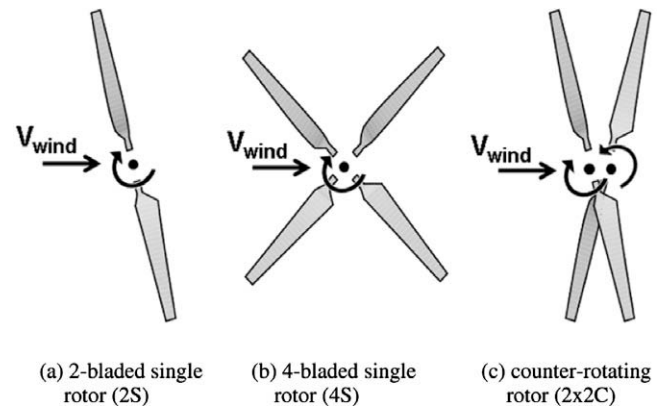


Fig. 2. Three kinds of rotor configurations.

Fig. 3 shows the radial distributions of  $a_{wake}$ . All trends of rotor configurations seem to be similar. All of  $a_{wake}$  increase gradually from  $r/R = 0.25$ , have maximum value at  $r/R = 0.70-0.75$  and decrease rapidly around  $r/R = 1.0$ . However, magnitudes of  $a_{wake}$  are different definitely. The main difference comes from the solidity of the rotor configurations.  $a_{wake}$  of 4S and 2 × 2C having the same solidity is about 1.7 times larger than that of 2S having the half of the solidity. Because larger  $a_{wake}$  generally means better performance of wind turbine, a rotor having a high solidity has an advan-

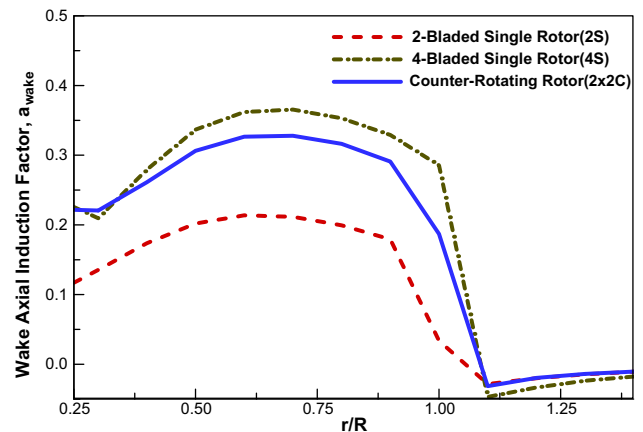


Fig. 3. Radial distributions of wake axial induction factors at TSR = 5.42, z/R = 0.3.

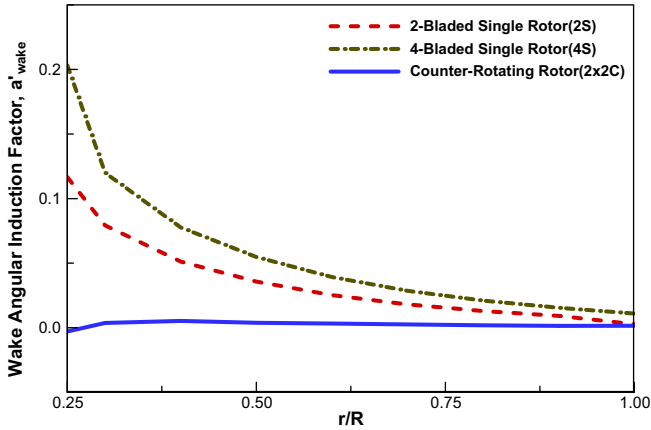


Fig. 4. Radial distributions of wake angular induction factors at TSR = 5.42,  $z/R = 0.3$ .

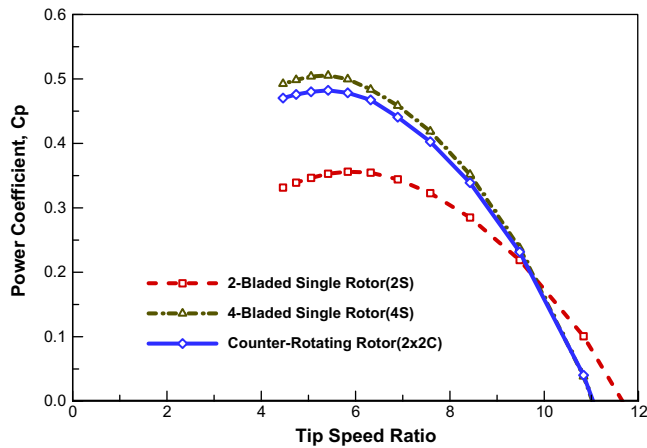


Fig. 5. Cp-TSR curve for each rotor configuration.

tage of aerodynamic performance. For the same solidity,  $a_{wake}$  of  $2 \times 2C$  are little lower than 4S. The reason is that efficiency of the rear rotor of  $2 \times 2C$  is reduced by interaction between front and rear rotor.

Fig. 4 depicts the radial distributions of  $a'_{wake}$ . Larger solidity gives larger value of  $a'_{wake}$ , except the  $2 \times 2C$  case. The reason  $a'_{wake}$  of  $2 \times 2C$  is nearly zero is that the swirl velocity induced by the front rotor is offset by the rear rotor rotating opposite direction. This phenomenon is the swirl recovery. Because swirl velocity of a wind turbine gives a disadvantage to performance, swirl recovery of a CRWT could be of help to the performance of wind turbine.

Power coefficients as function of TSR are shown in Fig. 5. The maximum  $C_p$  of 2S, 4S and  $2 \times 2C$  are about 0.36, 0.50 and 0.48, respectively. As the solidity increases, maximum  $C_p$  is increased by 30–40% of 2S and TSR corresponding to the maximum  $C_p$  decrease from 6 to 5.4. In addition, as the solidity increases, the  $C_p$  curves become to be steep.

The reason the TSR values decrease is that  $a_{wake}$  increases, as shown in Fig. 2. In other words, as  $a_{wake}$  increases, an effective angle of attack of rotor blades decreases and then larger wind speed is needed for the same rotating speed. Next, the reason of a steep  $C_p$  curve for higher solidity is that positive torque component induced by lift increases as the number of blades increases, but negative torque component induced by profile drag also in-

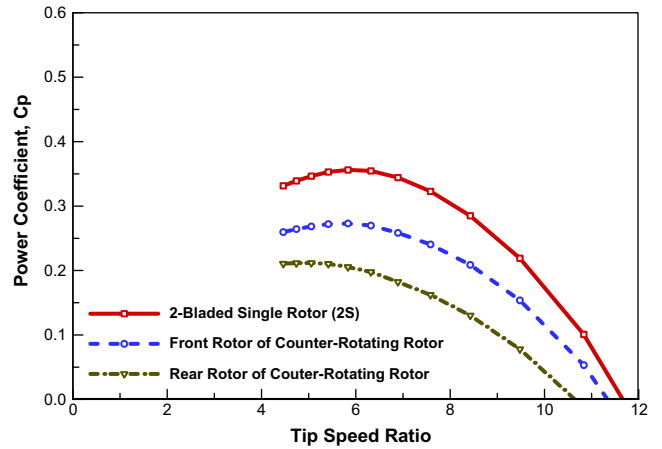


Fig. 6. Cp-TSR curve for 2-bladed rotors.

creases. In the large TSR region where the effects of lift components diminish, therefore,  $C_p$  for the rotors having higher solidity decrease rapidly.

For the rotors having the same solidity, maximum  $C_p$  of  $2 \times 2C$  is about 5% lower than that of 4S. This decrease comes from the interaction between front and rear rotor of  $2 \times 2C$  (Fig. 6). Though the  $2 \times 2C$  has an aerodynamic advantage of the swirl recovery, the adverse effect induced by the interaction is dominant, and the aerodynamic advantage occurred by swirl recovery is considered to hardly affect the performance of a wind turbine.

#### 4. Conclusions

In order to analyze the aerodynamic characteristics of a CRWT, three rotor configurations, 2-bladed single, 4-bladed single and counter-rotating rotor, were compared by using numerical method. The method used here was based on vortex lattice method and was validated with measurements of the NREL phase-VI rotor. The calculated shaft torque was found to be in good agreement with the experimental results.

The computations demonstrated that the wake axial induction factors increase as the solidity increase. However, due to the interaction of the rotors, the wake axial induction factor of a CRWT was shown to be little lower than that of a single rotor having equal solidity. In addition, the wake angular induction factor of a CRWT was shown to be nearly zero because the swirl velocity induced by the front rotor is offset by the rear rotor rotating opposite direction. Through the comparisons of maximum power coefficients, the efficiency of a CRWT was seen to be 30% more than a single rotor having half solidity and was shown to be 5% less than a single rotor having equal solidity. In addition, the aerodynamic advantage occurred by swirl recovery of a CRWT was demonstrated to hardly affect the performance of a wind turbine.

In this study, for a simple comparison, rotor configurations having equal rotating speed, pitch angle, swept area and blade geometry were compared. In order to improve a performance of a CRWT, a study for the variations of the previously mentioned parameters is necessary.

#### Acknowledgments

This work is the outcome of a Manpower Development Program for Energy and Resources supported by the Ministry of Knowledge and Economy (MKE) and was supported by Defense Acquisition Program Administration and Agency for Defense Development under the Contract UD070041AD.

## References

- [1] J.F. Manwell, J.G. McGowan, A.L. Rogers, *Wind Energy Explained, Theory, Design and Application*, John Wiley & Sons Ltd., 2002, pp. 84–88.
- [2] B.G. Newman, Actuator-disc theory for vertical-axis wind turbines, *J. Wind Eng. Ind. Aerodyn.* 15 (1983) 347–355.
- [3] K. Appa, Energy Innovations Small Grant (EISG) Program (Counter Rotating Wind Turbine System), EISG Final Report, California, US, 2002.
- [4] S. Jung, T. No, K. Ryu, Aerodynamic performance prediction of a 30 kW counter-rotating wind turbine system, *Renew. Energy* 30 (2005) 631–644.
- [5] W.Z. Shen, V.A.K. Zakkam, J.N. Sorensen, K. Appa, Analysis of counter-rotating wind turbines, *J. Phys., Conf. Ser.* 75 (2007).
- [6] J. Katz, A. Plotkin, *Low-Speed Aerodynamics*, Cambridge University Press, 2001, pp. 331–368.
- [7] S. Larwood, Wind turbine wake measurements in the operating region of a tail vane, in: *Proceedings of the 39th AIAA Aerospace Sciences Meeting*, Reno, Nevada, January 8–11, 2001.
- [8] C. Lindenburg, Investigation into Rotor Blade Aerodynamics – Analysis of the Stationary Measurements on the UAE Phase-VI Rotor in the NASA-Ames Wind Tunnel, ECN-C-03-025, 2003.